

Joint Spatial and Layer Attention for Convolutional Networks

Tony Joseph*, Konstantinos G. Derpanis**, Faisal Qureshi*,

{*University of Ontario Institute of Technology, **Ryerson University}, Canada

{tony.joseph, faisal.qureshi}@uoit.ca

Abstract

In this paper, we propose a novel approach that learns to sequentially attend to different Convolutional Neural Networks (CNN) layers (i.e., “what” feature abstraction to attend to) and different spatial locations of the selected feature map (i.e., “where”) to perform the task at hand. Specifically, at each Recurrent Neural Network (RNN) step, both a CNN layer and localized spatial region within it are selected for further processing. We demonstrate the effectiveness of this approach on two computer vision tasks: (i) image-based six degree of freedom camera pose regression and (ii) indoor scene classification. Empirically, we show that combining the “what” and “where” aspects of attention improves network performance on both tasks. We evaluate our method on standard benchmarks for camera localization (Cambridge, 7-Scenes, and TUM-LSI) and for scene classification (MIT-67 Indoor Scenes). For camera localization our approach reduces the median error by 18.8% for position and 8.2% for orientation (averaged over all scenes), and for scene classification it improves the mean accuracy by 3.4% over previous methods.

1. Introduction

Convolutional Neural Networks (CNNs) [25] are central models in a broad range of computer vision tasks, e.g., [23, 10, 9, 12, 26]. Generally, the processing of input imagery consists of a series of convolutional layers interwoven with non-linearities (and possibly downsampling) that yield a hierarchical image representation. As deterministic processing proceeds in a CNN, both the spatial scope (i.e., the effective receptive field) and the level of feature abstraction [31, 49] of the representation gradually increase. Motivated by our understanding of human visual processing [33, 40] and initial success in natural language processing [4], an emerging thread in computer vision research consists of augmenting CNNs with an attentional mechanism. Generally speaking, the goal of attention is to dynamically focus computational resources on the most salient features of the input image as dictated by the task.

In this paper, we present an approach that incorporates attention into a standard CNN in two ways: (i) a layer attention mechanism (i.e., “what” layer to consider) selects a CNN layer, and (ii) a spatial attention mechanism selects a spatial region within the selected layer (i.e., “where”) for subsequent processing. Layer and spatial attention work in conjunction with a Recurrent Neural Network (RNN). At each time step, first a layer is selected and next spatial attention is applied to it.

The RNN progressively aggregates the information from the attended spatial locations in the selected layers. The aggregated information is subsequently used for regression or classification. Our model is trained end-to-end, without requiring additional supervisory labels. Empirically, we consider both regression (i.e., six degree of freedom, 6-DoF, camera localization) and classification (i.e., scene classification) tasks. Figure 1 presents an overview of our approach to layer-spatial attention for 6-DoF camera localization.

The guiding intuition behind our approach is that the optimal feature set for a task may be distributed across a variety of feature abstraction levels and spatial regions. Here, we let an RNN identify the optimal features to aggregate. For instance, in the context of image-based localization, a scene may contain both a set of salient objects captured by high-level features, such as a window or door, and texture-like regions captured by low-level features. Prior localization methods have exclusively relied on either low-level features (e.g., [44]) or high-level ones, e.g., [2, 21]. Our approach considers the spectrum of feature abstractions in a unified manner.

1.1. Contributions

This paper makes the following contributions:

1. We propose an attention model that learns to sequentially attend to different CNN layers (i.e., different levels of abstraction) and different spatial locations (i.e., specific regions within the selected feature map) to perform the task at hand.
2. We augment a standard CNN architecture, GoogLeNet [38], with our attention model and empirically demon-

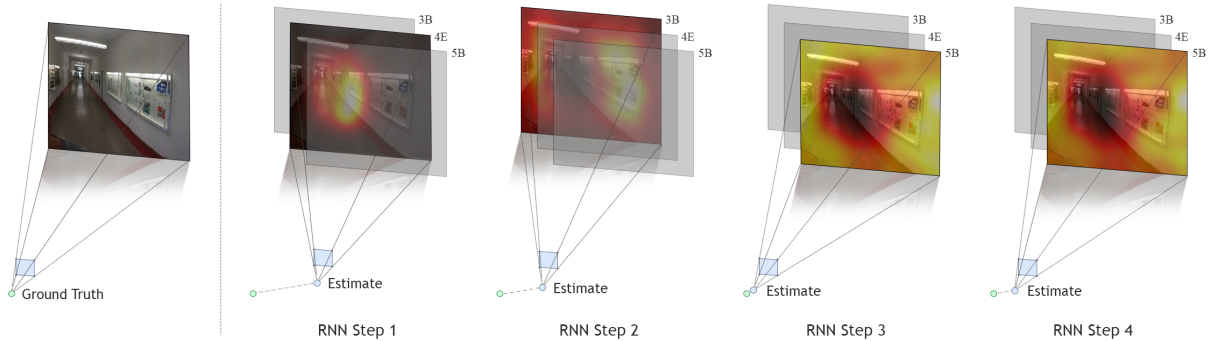


Figure 1: Overview of our approach to 6-DoF camera localization. Given a set of CNN feature layers (GoogLeNet [38] Conv- $\{3B, 4C, 4E, 5B\}$ layers shown) our approach to attention uses an RNN to sequentially select a set of feature layers (highlighted by the non-grey images) and corresponding locations in the layers (highlighted by the heat maps). Finally, the processed attended features are used for regressing the camera position and orientation.

strate its efficacy on both regression and classification tasks: 6-DoF camera localization regression and indoor scene classification. We evaluate the proposed architecture on standard benchmarks: (a) Cambridge Landmarks, 7 Scenes, and TU Munich Large-Scale Indoor (TUM-LSI) for camera pose estimation; and (b) MIT-67 Indoor Scenes for scene classification. For camera localization our approach reduced the overall median error by 12.3% for position and 13.9% for orientation on Cambridge Landmarks, 19.3% for position and 8.83% for orientation on 7-Scenes, and 25.1% for position and 1.79% for orientation on TUM-LSI over the baseline [42]. For indoor scene classification on MIT-67 [32] our approach improves the mean accuracy by 3.4% over the baseline [8]. In both tasks, the baseline methods use the *same* base convolutional network.

2. Related works

2.1. Attention.

Attention is a mechanism that dynamically allocates computational resources to the most salient features of the input signal. Attention has appeared in a variety of recent architectures [24, 48, 39, 3, 30, 16, 41]. A natural way to implement a sequential attentional probing mechanism is with a Recurrent Neural Network (RNN) or variant (e.g., Long Short-Term Memory, LSTM [11, 48]) in conjunction with a gating function [37, 43, 46] that yields a soft (e.g., softmax or sigmoid) or hard attention [47, 45]. The attentional policy is learned without an explicit training signal, rather the task-related loss alone provides the training signal for the attention-related weights. In this work, we incorporate both soft (spatial selection) and hard (layer selection) attention in an end-to-end trainable architecture. Most

closely related to the current work are the soft and hard selection mechanisms proposed by Xu *et al.* [47] and Veit and Belongie [41], respectively. Xu *et al.* [47] proposed an end-to-end trainable soft spatial attention architecture for image captioning. We adapt this soft attention architecture for our purposes and further extend it to include hard attention. Veit and Belongie [41] proposed a dynamic convolutional architecture that selects whether or not information propagates through a given CNN layer during a forward pass. Similar to Veit and Belongie [41], we use the recently proposed Gumbel-Softmax to realize our discrete (hard) selection of layers.

2.2. Image-based camera pose localization.

Low-level features (e.g., SIFT [28]) have dominated the camera pose localization literature, e.g., [2, 34, 27, 6]. An early example of using high-level features for camera localization appeared in Anati *et al.* [2], where heatmaps from object detections were used for localization. More recently, high-level CNN features have garnered attention. These features can be considered as soft proxies to object detections. Kendall *et al.* [21, 18] proposed PoseNet, an image-based 6-DoF camera localization method. PoseNet regresses the camera position and orientation based on input provided by a CNN layer Kendall and Cipolla [19] reconsidered the loss used in PoseNet to integrate additional geometric information. Walch *et al.* [42] extended the PoseNet approach by introducing an LSTM-based dimensionality reduction step prior to regression to avoid overfitting. In each case, the networks rely on features from a manually selected layer, located relatively high in the feature hierarchy. In contrast, we propose an attentional network that is capable of dynamically integrating the most salient features across the spectrum of feature abstractions (capturing potentially texture-like and object-related features as necessary).

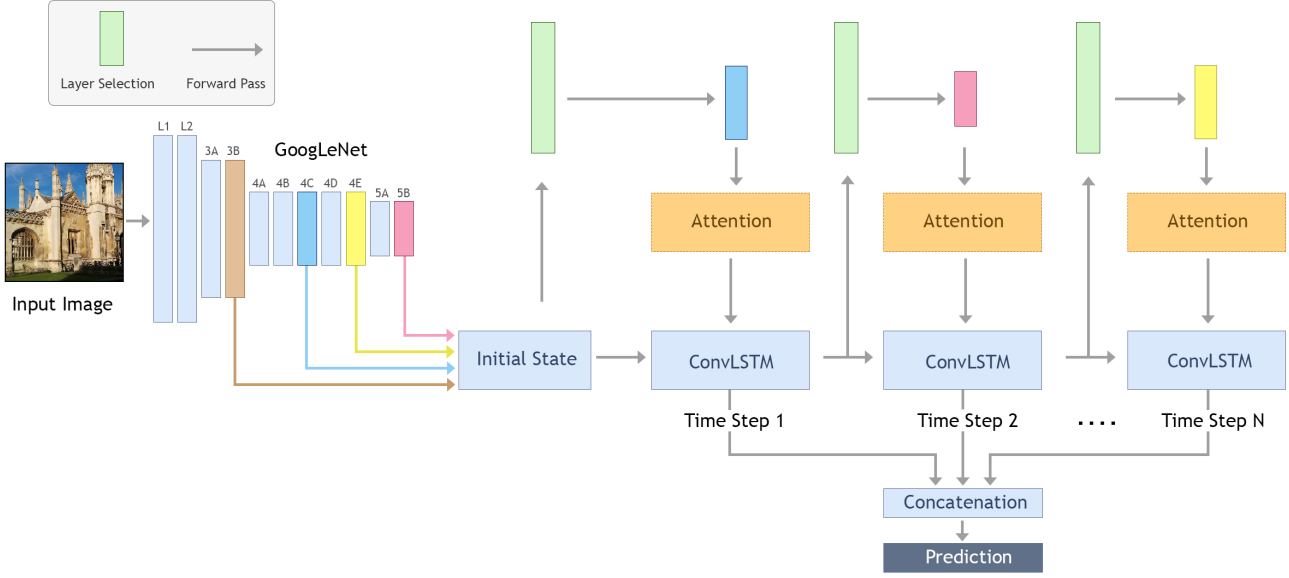


Figure 2: Overview of our layer-spatial attention architecture. Layer-spatial attention is realized within a Conv-LSTM framework, where the layer attention uses the previous hidden state, and spatial attention uses both the selected layer and the previous hidden state. After N Conv-LSTM steps, the hidden states from all steps are concatenated and used for regression or classification.

2.3. Indoor scene classification.

To demonstrate the generality of our approach we also consider a classification task, indoor scene classification. Here, a wealth of research has considered both handcrafted (e.g., [5, 17]) and learned deep features, e.g., [35, 8]. In this work, we compare our approach using a standard deep architecture, GoogLeNet [38], which we also use as the base network for our layer-spatial attention method.

3. Technical approach

Our layer-spatial attention network sequentially probes the input signal over a fixed number of steps. It is comprised of a hard selection mechanism that selects a CNN layer (Sec. 3.2) and soft attention that selects a spatial location within the selected layer (Sec. 3.1). The attention network is realized using a convolutional LSTM (Conv-LSTM) [46]. Figure 2 provides an overview of our architecture. At each Conv-LSTM step, the layer attention selects a CNN layer and spatial attention localizes a region within it. After N recurrent steps, the Conv-LSTM hidden states for all steps are concatenated and used for classification or regression.

3.1. Where: Spatial attention

We adapt the recurrent model from Xu *et al.* [47] with soft spatial attention as the foundation of our method. At each time step t , the spatial attention mechanism receives

as input the selected layer $\mathbf{f} \in \mathbb{R}^{h_f \times w_f \times d_f}$ (see Sec. 3.2) and the recurrent hidden state $\mathbf{h}_t \in \mathbb{R}^{h_h \times w_h \times d_h}$ from the previous step. The soft attention layer is implemented as follows:

$$\begin{aligned} \mathbf{h}_{att} &= \mathbf{h}_t * \mathbf{E}_h \\ \mathbf{f}_{att} &= \text{ReLU}(\mathbf{h}_{att} + \mathbf{f}) \\ \mathbf{O}_{att} &= \text{softmax}(\mathbf{f}_{att} * \mathbf{C}_A) \odot \mathbf{f}, \end{aligned} \quad (1)$$

where $*$ denotes the convolutional operator and \odot is element-wise multiplication. The attention layer consists of two convolutional layers, \mathbf{E}_h and \mathbf{C}_A , which compute an embedding and (unscaled) attention mask, respectively. The embedding layer, \mathbf{E}_h , is used to transform the hidden state channel dimension to bring it equal to the input layer’s channel dimension. The \mathbf{C}_A layer computes the unscaled attention mask with dimensions $h_f \times w_f \times 1$. The final attention mask is computed by taking the softmax of the unscaled attention mask. The output of the attention layer \mathbf{O}_{att} is obtained by taking an element-wise multiplication between the features in each channel and attention map.

3.2. What: Layer attention

In layer attention (i.e., “what” features to attend) a CNN layer is selected whose feature map is deemed to contain the most salient information at the current recurrent step. Our layer attention involves a discrete (hard) selection of a CNN

layer. Here, we use the recently proposed continuous relaxation of the Gumbel-Max trick [7], the Gumbel-Softmax [29, 15], to realize the discrete selection of layers.

Gumbel-Max provides a simple and efficient way to draw samples from a categorical (discrete) distribution:

$$z = \text{one_hot}(\arg \max [g_i + \log \pi_i]), \quad (2)$$

where, g_1, \dots, g_k are i.i.d. samples drawn from the Gumbel(0, 1) distribution, and π_i are unnormalized probabilities. Samples g are drawn using the following procedure: (i) draw sample $u \sim \text{Uniform}(0, 1)$; and (ii) set $g = -\log(-\log(u))$. In the forward pass (and during testing), we compute the arg max of the unnormalized probabilities. In contrast, in the backward pass the arg max is approximated with a softmax function:

$$y_i = \frac{\exp\left(\frac{\log(\pi_i) + g_i}{\tau}\right)}{\sum_{j=1}^k \exp\left(\frac{\log(\pi_j) + g_j}{\tau}\right)}, \quad (3)$$

where k is the number of CNN layers that are considered for selection, $i \in [1, k]$, and τ represents temperature. (This approach is the straight-through version of the Gumbel-Softmax estimator proposed in [15].) During training the temperature, τ , is progressively lowered. As the temperature approaches zero, samples from the Gumbel-Softmax distribution closely approximate those drawn from a categorical distribution.

For layer attention, we realize the (layer) selection scores (i.e., unnormalized probabilities) at each recurrent step as the output of a fully connected layer computed using the previous hidden state. During the forward pass we perform layer selection using Eq. 2 and in the backward pass gradients are computed using Eq. 3 to keep our architecture end-to-end trainable.

3.3. Tasks

In our approach, after N Conv-LSTM steps, the hidden states are concatenated, average pooled, and passed onto a fully connected layer for (regression/classification) prediction. To ensure that our comparisons are meaningful, and that any differences in the performance of our method to those posted by previous methods are due to our attention mechanism, we use the exact same losses as those used by our baselines.

3.3.1 Camera pose estimation

The proposed camera localization network takes an RGB image as input and outputs camera position and orientation $[\hat{\mathbf{x}}, \hat{\mathbf{q}}]^\top$. Camera pose is defined relative to an arbitrary reference frame. We use the same regression loss as our

baselines [21, 20, 42] to facilitate direct empirical comparison:

$$\mathcal{L} = \|\mathbf{x} - \hat{\mathbf{x}}\|_2 + \beta \|\mathbf{q} - \frac{\hat{\mathbf{q}}}{\|\hat{\mathbf{q}}\|_2}\|_2, \quad (4)$$

where $[\mathbf{x}, \mathbf{q}]^\top$ represent ground truth position \mathbf{x} and orientation \mathbf{q} , and $[\hat{\mathbf{x}}, \hat{\mathbf{q}}]^\top$ denote predicted position $\hat{\mathbf{x}}$ and orientation $\hat{\mathbf{q}}$. Orientations are represented using quaternions. β is a scalar hyperparameter that determines the relative weighting between the positional and orientation errors. We use the same β value as our baselines, PoseNet [21] and LSTM-PoseNet [42].

3.3.2 Indoor scene classification

Consistent with our scene classification baseline [38], we use the standard cross-entropy classification loss:

$$\mathcal{L} = -\mathbf{y}_c^\top \log(\hat{\mathbf{y}}_c), \quad (5)$$

where \mathbf{y}_c is a one-hot encoded class label for class c , and $\hat{\mathbf{y}}_c$ is the output of the softmax classifier.

3.4. Implementation details

To realize our layer-spatial attention model we use the same basic architecture as Xu *et al.* [47] for sequential spatial attention. We augment this network with hard attention for layer selection. To avoid overfitting, we replace the LSTM layers with ConvLSTM [46] layers that reduce the network weight parameterization. The hidden state size is set to 96. In this work we used a multi-convolutional layer modeled after the Inception module [38] for layer-spatial selection; see the supplementary material for further discussion. All experiments use GoogLeNet [38] as the feature extractor to maintain meaningful comparisons with the baseline methods. It is conceivable that using a different base network may yield improved results; however, the focus of our experiments is to study the impact of our proposed layer-spatial attention mechanism.

For practical reasons we selected a sparse set of layers (Conv- $\{3B, 4C, 4E, 5B\}$) that capture a range of abstractions. It is straightforward to extend the network to select any layer; however, it will considerably increase the training time. Another consideration is that the layers often have different channel dimensions, which necessitates additional weights for embedding layers. All models were trained end-to-end using the ADAM [22] optimizer. Batch-Norm [13] with default parameters is applied to both spatial attention and layer selection network. Our code is implemented using TensorFlow 1.4 [1]. Additional details about our architecture are provide in the supplementary material.

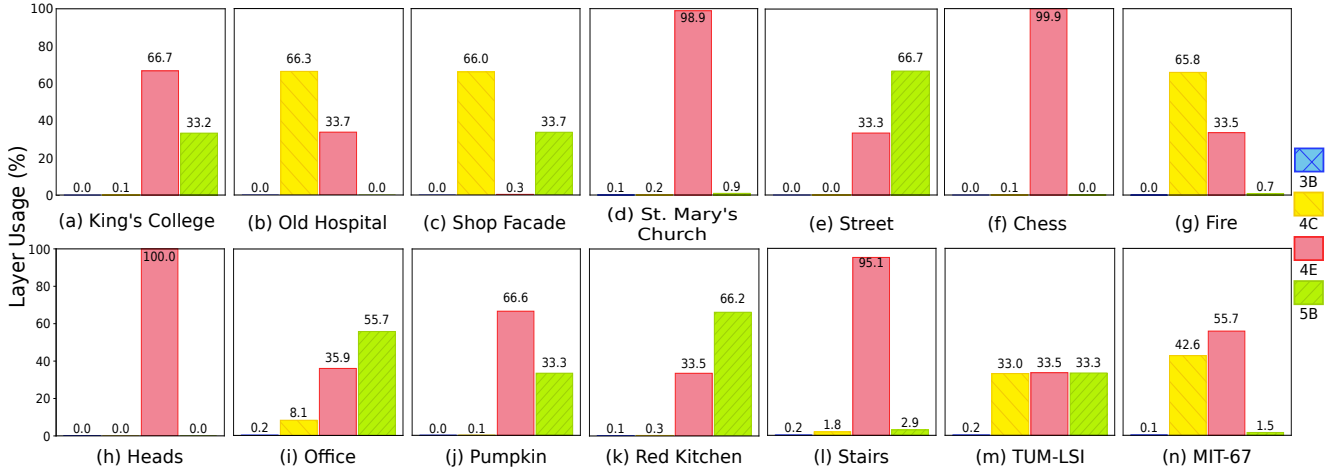


Figure 3: Layer Selection Frequencies (LSF) on all four datasets on the test set. (a) - (e) are Cambridge Landmarks scenes, (f) - (l) are scenes from 7-Scenes, (m) and (n) are TUM-LSI, and MIT-67 dataset, respectively. The bins refer to the GoogLeNet[38] Conv- $\{3B, 4C, 4E, 5B\}$ layers. The vertical axis represents layer usage percentages.

4. Empirical evaluation

4.1. Datasets

We evaluate our layer-spatial attention model on a variety of standard datasets. For 6-DoF camera localization we evaluate on Cambridge Landmarks [21], 7-Scenes [36], and TUM-LSI [42]. For scene classification we evaluate on MIT-67 Indoor Scenes [32]. (Additional information on these datasets can be found in the supplementary materials.) For camera pose estimation, we resize the images to 256×455 pixels. As done in our localization baselines [21, 42], separate mean images are computed for each colour channel and the images are mean subtracted per channel. For indoor scene classification, we resize the images to 256×256 . For all experiments, we use crops of 224×224 pixels (random crops during training and center crops during testing). For indoor scene classification we also used random horizontal flips during training.

4.2. Results

Figure 3 shows the frequencies of the GoogLeNet feature layers selected for each dataset on the respective test sets. As can be seen, the datasets predominately utilize more than one layer. Furthermore, the layers most frequently selected differ widely amongst the datasets. We found that for image-based camera localization using three Conv-LSTM steps worked best, after which the performance decreases, the error increases. In the case of indoor scene classification two Conv-LSTM steps performed best. Additional experiments using five recurrent steps are shown in the supplementary materials for both tasks.

Camera localization. Table 1 compares our proposed

method against image-based camera pose regression methods [21, 18, 42]. All the compared methods use GoogLeNet as the source of features for regression, with the baselines limiting features to layer Conv-5B. In terms of the individual scenes, our method achieves the least error in both translation and rotation in the majority of cases at three steps. Considering the aggregate results over the respective datasets, we see our method yields significant improvements over the state-of-the-art, ranging between 12.3 and 25.1 percent for translation and 1.79 and 13.9 percent for rotation.

The TUM-LSI dataset contains large textureless surfaces and repetitive scene elements covering over $5,575 m^2$. Active search or SIFT-based approaches have been previously shown to perform poorly on this dataset [42]. Our method achieves state-of-the-art performance, suggesting that the ability to attend to different CNN layers over successive LSTM steps helps. Figure 4 (top row) shows qualitative results for camera localization. For outdoor scenes, it appears our attention mechanism captures both low-level (e.g., corners) and high-level structures (e.g., rooftops and windows).

Indoor scene classification. Table 8 compares our proposed layer-spatial attention method against three baselines [35, 8, 38]. The proposed method achieves best performance after two recurrent steps. Figure 4 (bottom row) shows several qualitative results for indoor scene classification. The layer-spatial attention seems to capture objects and physical scene structures present in the scene. For the Concert Hall image, the attention mechanism appears to focus on the entire image, perhaps focusing on the scene architecture. For the Dental Office image, spatial attention picks out the dental equipment (a permanent fixture) and

Dataset	Area or Volume	PoseNet [21]	Bayesian PoseNet [20]	LSTM PoseNet [42]	Ours			
					Conv-LSTM Step-1	Conv-LSTM Step-2	Conv-LSTM Step-3	Improvement (meter, degree)
Great Court	8000 m^2	-	-	-	-	-	-	-
Kings College	5600 m^2	1.66 m, 4.86°	1.74 m, 4.06°	0.99 m, 3.65°	1.02 m, 4.22°	1.00 m, 4.51°	0.90 m, 3.70°	+9.09, -1.36
Old Hospital	2000 m^2	2.62 m, 4.90°	2.57 m, 5.14°	1.51 m, 4.29°	1.62 m, 4.11°	1.51 m, 4.02°	1.36 m, 3.95°	+9.93, +7.92
Shop Facade	875 m^2	1.41 m, 7.18°	1.25 m, 7.54°	1.18 m, 7.44°	1.15 m, 5.45°	0.95 m, 6.44°	0.91 m, 5.29°	+22.8, +28.8
St. Marys Church	4800 m^2	2.45 m, 7.96°	2.11 m, 8.38°	1.52 m, 6.68°	1.62 m, 7.22°	1.59 m, 5.94°	1.42 m, 6.07°	+6.57, +1.64
Street	50000 m^2	-	-	-	18.7m, 34.1°	15.0 m, 30.3°	13.9 m, 30.0°	-
Average [42]	3319 m^2	2.08 m, 6.83°	1.92 m, 6.28°	1.30 m, 5.52°	1.35 m, 5.25°	1.26 m, 5.22°	1.14 m, 4.75°	+12.3, +13.9
Chess	6.0 m^3	0.32 m, 6.08°	0.37 m, 7.24°	0.24 m, 5.77°	0.17 m, 5.58°	0.16 m, 5.27°	0.15 m, 4.79°	+37.5, +16.9
Fire	2.5 m^3	0.47 m, 14.0°	0.43 m, 13.7°	0.34 m, 11.9°	0.32 m, 12.6°	0.31 m, 11.7°	0.23 m, 10.0°	+32.3, +15.9
Heads	1.0 m^3	0.30 m, 12.2°	0.31 m, 12.0°	0.21 m, 13.7°	0.18 m, 13.8°	0.18 m, 14.1°	0.18 m, 13.7°	+14.2, +0.00
Office	7.5 m^3	0.48 m, 7.24°	0.48 m, 8.04°	0.30 m, 8.08°	0.29 m, 7.63°	0.29 m, 7.23°	0.29 m, 8.02°	+3.33, +0.74
Pumpkin	5.0 m^3	0.49 m, 8.12°	0.61 m, 7.08°	0.33 m, 7.00°	0.25 m, 5.46°	0.25 m, 5.76°	0.26 m, 6.16°	+21.2, +12.0
Red Kitchen	18 m^3	0.58 m, 8.31°	0.58 m, 7.51°	0.37 m, 8.83°	0.43 m, 8.03°	0.37 m, 7.49°	0.39 m, 8.20°	-2.00, +5.77
Stairs	7.5 m^3	0.48 m, 13.1°	0.48 m, 13.1°	0.40 m, 13.7°	0.32 m, 9.98°	0.31 m, 10.5°	0.29 m, 12.0°	+27.5, +12.4
Average All	6.9 m^3	0.44 m, 9.01°	0.46 m, 9.81°	0.31 m, 9.85°	0.28 m, 9.01°	0.26 m, 8.86°	0.25 m, 8.98°	+19.1, +9.10
TUM-LSI	5575 m^2	1.87 m, 6.14°	-	1.31 m, 2.79°	1.32 m, 3.82°	1.26 m, 3.69°	0.98 m, 2.74°	+25.1, +1.79

Table 1: Camera localization results. Median localization error achieved by the proposed attention model over three steps on Cambridge Landmarks, 7-Scenes, and TUM-LSI. Bold values indicate the lowest error achieved for each row. Improvement is reported with respect to LSTM-PoseNet [42]. A dash (-) indicates that no result is reported.

CNNaug-SVM [35]	S ² ICA [8]	GoogLeNet [38]	Ours			
			Conv-LSTM Step-1	Conv-LSTM Step-2	Conv-LSTM Step-3	Improvement (%)
69.0 %	71.2 %	73.7 %	74.5 %	77.1 %	76.0 %	+3.4

Table 2: Mean accuracy results for indoor scene classification on MIT-67. The proposed method achieves the highest accuracy (shown in boldface). Improvement is reported with respect to the GoogLeNet [38] baseline.

correctly ignores the person (a transient entity). For the Closet image, clothes and cabinetry are selected. Finally, for the Gym image, the proposed attention mechanism selects the exercise equipment.

4.3. Ablation study

Table 3 summarizes an ablation study that we performed to gauge the impact of combining layer selection with spatial attention. We choose Old Hospital (Cambridge Landmarks), Office (7-Scenes), TUM-LSI, and MIT-67 datasets for this ablation study. Old Hospital and Office were selected since we found these to be the most challenging for our proposed network.

We manually selected GoogLeNet’s Conv- $\{3B, 4E, 5B\}$

layers and applied spatial attention to each independently. (Note, the PoseNet results reported in Table 1 use layer Conv-5B without any form of attention for direct position-orientation regression.) Our results confirm that it is sometimes beneficial to use layers other than the final CNN layer. Median localization errors, for example, improve for both Old Hospital and Office datasets when we use layers other than Conv-5B. Note that in previous camera pose localization works [21, 18, 42] Conv-5B was manually selected. For indoor scene classification, selecting Conv-4E yields the best result. The last column of Table 3 includes results obtained by combining layer selection and spatial attention. Notice that in three out of four cases shown, network achieves best performance (lowest errors in case of

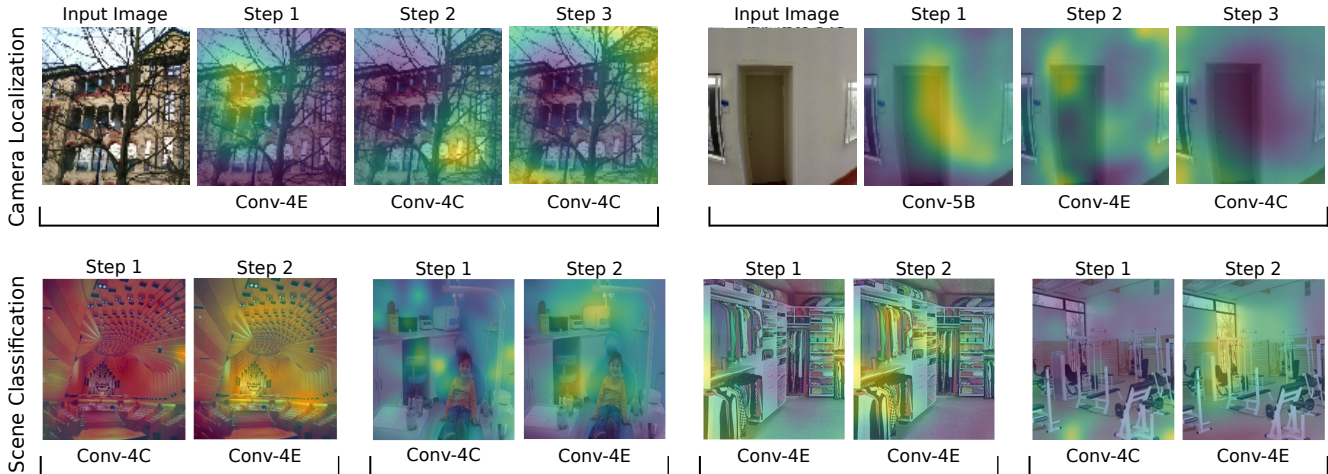


Figure 4: Qualitative results on camera pose localization (top row) and indoor scene classification (bottom row). Top row: input image along with the spatial attention superimposed on the input image for three Conv-LSTM steps. Bottom row: spatial attention superimposed on the input image for two Conv-LSTM steps. The labels underneath each image indicates the selected CNN layer.

Dataset	Spatial Attention Only			Layer Selection Only	Spatial and Layer Attention
	Conv-3B	Conv-4E	Conv-5B		
Camera-Pose Estimation					
Old Hospital	1.49 m, 4.29°	1.42 m, 4.37°	1.76 m, 4.44°	2.36 m, 6.28°	1.36 m, 3.95°
Office	0.27 m, 7.37°	0.26 m, 7.35°	0.28 m, 7.52°	0.33 m, 7.97°	0.29 m, 8.02°
TUM-LSI	1.21 m, 3.26°	1.13 m, 3.66°	1.12 m, 3.66°	5.27 m, 10.8°	0.98 m, 2.74°
Indoor-Scene Classification					
MIT-67	61.6 %	74.5 %	74.2 %	76.4 %	77.1 %

Table 3: Ablation study on layer-spatial attention. In all cases, GoogLeNet [38] Conv- $\{3B, 4E, 5B\}$ layers are used. Bold values indicate the best result achieved for each row.

camera pose estimation, and highest accuracy in case of indoor scene classification) when using both layer selection and spatial attention. The second last column in Table 3 includes results when using layer selection alone. The network performance deteriorates when spatial attention is absent.

Our results are consistent with our initial guiding intuition that salient information is distributed across the spectrum of feature abstractions, e.g., things vs. stuff. Our proposed layer-spatial attention mechanism exploits this aspect to achieve better performance.

5. Conclusion

In this paper, we have presented an architecture that dynamically probes the convolutional layers of a CNN to ag-

gregate and process the optimal set of features for a given task. We introduced an attention architecture that learns to sequentially attend to different CNN layers (i.e., levels of feature abstraction) and different spatial locations within the selected layer. In the context of two vision tasks, camera localization and scene classification, we empirically showed that our approach to layer-spatial attention improves regression and classification performance over manually selecting layers and previous approaches. Our proposed approach to attention is general and may prove useful for other vision tasks.

6. Acknowledgments

The authors would like to thank Kamyar Nazari (Imaging lab, University of Ontario Institute of Technology,

Canada) for providing support on figures presented in this paper. We gratefully acknowledge the support of NVIDIA Corporation with the donation of the Titan Xp GPU used for this research.

References

- [1] M. Abadi, A. Agarwal, P. Barham, E. Brevdo, Z. Chen, C. Citro, G. S. Corrado, A. Davis, J. Dean, M. Devin, S. Ghemawat, I. Goodfellow, A. Harp, G. Irving, M. Isard, Y. Jia, R. Jozefowicz, L. Kaiser, M. Kudlur, J. Levenberg, D. Mané, R. Monga, S. Moore, D. Murray, C. Olah, M. Schuster, J. Shlens, B. Steiner, I. Sutskever, K. Talwar, P. Tucker, V. Vanhoucke, V. Vasudevan, F. Viégas, O. Vinyals, P. Warden, M. Wattenberg, M. Wicke, Y. Yu, and X. Zheng. TensorFlow: A System For Large-Scale Machine Learning. *Proc. of the Operating Systems: Design and Implementation (OSDI)*, 16:265–283, 2016. 4
- [2] R. Anati, D. Scaramuzza, K. G. Derpanis, and K. Daniilidis. Robot Localization Using Soft Object Detection. In *Proc. of the IEEE Conference on International Conference on Robotics and Automation (ICRA)*, pages 4992–4999, 2012. 1, 2
- [3] J. Ba, V. Mnih, and K. Kavukcuoglu. Multiple Object Recognition with Visual Attention. In *Proc. of the IEEE Conference on International Conference on Robotics and Automation (ICRA)*, 2015. 2
- [4] D. Bahdanau, K. Cho, and Y. Bengio. Neural Machine Translation by Jointly Learning to Align and Translate. In *Proc. of the International Conference on Learning Representations (ICLR)*, 2015. 1
- [5] C. Doersch, A. Gupta, and A. A. Efros. Mid-level visual element discovery as discriminative mode seeking. In *Proc. of Advances in Neural Information Processing Systems (NeurIPS)*, pages 494–502, 2013. 3
- [6] J. Engel, T. Schöps, and D. Cremers. LSD-SLAM: Large-scale direct monocular SLAM. In *Proc. of the European Conference on Computer Vision (ECCV)*, pages 834–849, 2014. 2
- [7] E. J. Gumbel. *Statistical theory of extreme values and some practical applications: a series of lectures*. US Govt. Print. Office, 21954. 4
- [8] M. Hayat, S. H. Khan, M. Bennamoun, and S. An. A Spatial Layout and Scale Invariant Feature Representation for Indoor Scene Classification. *Proc. of the IEEE Transactions on Image Processing*, pages 4829–4841, 2016. 2, 3, 5, 6, 16
- [9] K. He, G. Gkioxari, P. Dollár, and R. Girshick. Mask R-CNN. In *Proc. of the IEEE Conference on International Conference on Computer Vision (ICCV)*, pages 2980–2988, 2017. 1
- [10] K. He, X. Zhang, S. Ren, and J. Sun. Deep Residual Learning for Image Recognition. In *Proc. of the IEEE Conference on Computer Vision and Pattern Recognition (CVPR)*, pages 770–778, 2016. 1
- [11] S. Hochreiter and J. Schmidhuber. Long Short-Term Memory. *Neural Computation*, 9(8):1735–1780, 1997. 2
- [12] E. Ilg, N. Mayer, T. Saikia, M. Keuper, A. Dosovitskiy, and T. Brox. FlowNet 2.0: Evolution of optical flow estimation with deep networks. In *Proc. of the IEEE Conference on Computer Vision and Pattern Recognition workshops (CVPR)*, pages 1647–1655, 2017. 1
- [13] S. Ioffe and C. Szegedy. Batch Normalization: Accelerating Deep Network Training by Reducing Internal Covariate Shift. In *Proc. of the International Conference on Machine Learning (ICML)*, pages 448–456, 2015. 4
- [14] S. Izadi, D. Kim, O. Hilliges, D. Molyneaux, R. Newcombe, P. Kohli, J. Shotton, S. Hodges, D. Freeman, A. Davison, et al. Kinectfusion: real-time 3d reconstruction and interaction using a moving depth camera. In *Proc. of the ACM symposium on User interface software and technology*, pages 559–568, 2011. 11
- [15] E. Jang, S. Gu, and B. Poole. Categorical Reparameterization with Gumbel-Softmax. In *Proc. of the International Conference on Learning Representations (ICLR)*, 2017. 4
- [16] D. Jayaraman and K. Grauman. Learning to look around: Intelligently exploring unseen environments for unknown tasks. *CoRR*, abs/1709.00507:1–11, 2017. 2
- [17] M. Juneja, A. Vedaldi, C. Jawahar, and A. Zisserman. Blocks that shout: Distinctive parts for scene classification. In *Proc. of the IEEE Conference on Computer Vision and Pattern Recognition (CVPR)*, pages 923–930, 2013. 3
- [18] A. Kendall and R. Cipolla. Modelling uncertainty in deep learning for camera relocalization. In *Proc. of the IEEE Conference on International Conference on Robotics and Automation (ICRA)*, pages 4762–4769, 2016. 2, 5, 6
- [19] A. Kendall, R. Cipolla, et al. Geometric loss functions for camera pose regression with deep learning. In *Proc. of the IEEE Conference on Computer Vision and Pattern Recognition (CVPR)*, pages 8–16, 2017. 2
- [20] A. Kendall and Y. Gal. What uncertainties do we need in bayesian deep learning for computer vision? In *Proc. of Advances in Neural Information Processing Systems (NeurIPS)*, pages 5574–5584, 2017. 4, 6, 16

- [21] A. Kendall, M. Grimes, and R. Cipolla. PoseNet: A Convolutional Network for Real-Time 6-DOF Camera Relocalization. In *Proc. of the IEEE Conference on Computer Vision and Pattern Recognition (CVPR)*, pages 2938–2946, 2015. 1, 2, 4, 5, 6, 11, 12, 13, 14, 16
- [22] D. P. Kingma and J. Ba. Adam: A Method for Stochastic Optimization. In *Proc. of the International Conference on Learning Representations (ICLR)*, 2015. 4
- [23] A. Krizhevsky, I. Sutskever, and G. E. Hinton. Imagenet Classification with Deep Convolutional Neural Networks. In *Proc. of Advances in Neural Information Processing Systems (NeurIPS)*, pages 1097–1105, 2012. 1
- [24] H. Larochelle and G. E. Hinton. Learning to combine foveal glimpses with a third-order boltzmann machine. In *Proc. of Advances in Neural Information Processing Systems (NeurIPS)*, pages 1243–1251, 2010. 2
- [25] Y. LeCun, B. E. Boser, J. S. Denker, D. Henderson, R. E. Howard, W. E. Hubbard, and L. D. Jackel. Handwritten digit recognition with a back-propagation network. In *Proc. of Advances in Neural Information Processing Systems (NeurIPS)*, pages 396–404, 1990. 1
- [26] C. Ledig, L. Theis, F. Huszár, J. Caballero, A. Cunningham, A. Acosta, A. P. Aitken, A. Tejani, J. Totz, Z. Wang, et al. Photo-realistic single image super-resolution using a generative adversarial network. In *Proc. of the IEEE Conference on Computer Vision and Pattern Recognition workshops (CVPR)*, pages 105–114, 2017. 1
- [27] Y. Li, N. Snavely, D. Huttenlocher, and P. Fua. World-wide Pose Estimation using 3D Point Clouds. In *Proc. of the European Conference on Computer Vision (ECCV)*, pages 15–29, 2012. 2
- [28] D. G. Lowe. Distinctive Image Features from Scale-Invariant Keypoints. *International Journal of Computer Vision (IJCV)*, 60(2):91–110, 2004. 2
- [29] C. J. Maddison, D. Tarlow, and T. Minka. A* sampling. In *Proc. of Advances in Neural Information Processing Systems (NeurIPS)*, pages 3086–3094, 2014. 4
- [30] V. Mnih, N. Heess, A. Graves, and K. Kavukcuoglu. Recurrent Models of Visual Attention. In *Proc. of Advances in Neural Information Processing Systems (NeurIPS)*, pages 2204–2212, 2014. 2
- [31] C. Olah, A. Mordvintsev, and L. Schubert. Feature Visualization. *Distill*, 2017. <https://distill.pub/2017/feature-visualization>. 1
- [32] A. Quattoni and A. Torralba. Recognizing indoor scenes. In *Proc. of the IEEE Conference on Conference on Computer Vision and Pattern Recognition (CVPR)*, pages 413–420, 2009. 2, 5, 11
- [33] R. A. Rensink. The Dynamic Representation of scenes. *Visual Cognition*, 7:17–42, 2000. 1
- [34] T. Sattler, B. Leibe, and L. Kobbelt. Efficient & Effective Prioritized Matching for Large-Scale Image-Based Localization. *Transactions on Pattern Analysis and Machine Intelligence (PAMI)*, 39(9):1744–1756, 2017. 2
- [35] A. Sharif Razavian, H. Azizpour, J. Sullivan, and S. Carlsson. Cnn features off-the-shelf: an astounding baseline for recognition. In *Proc. of the IEEE Conference on Computer Vision and Pattern Recognition workshops (CVPR)*, pages 806–813, 2014. 3, 5, 6, 16
- [36] J. Shotton, B. Glocker, C. Zach, S. Izadi, A. Criminisi, and A. Fitzgibbon. Scene coordinate regression forests for camera relocalization in rgb-d images. In *Proc. of the IEEE Conference on Conference on Computer Vision and Pattern Recognition (CVPR)*, pages 2930–2937, 2013. 5, 11
- [37] M. F. Stollenga, J. Masci, F. J. Gomez, and J. Schmidhuber. Deep Networks with Internal Selective Attention through Feedback Connections. In *Proc. of Advances in Neural Information Processing Systems (NeurIPS)*, pages 3545–3553, 2014. 2
- [38] C. Szegedy, W. Liu, Y. Jia, P. Sermanet, S. E. Reed, D. Anguelov, D. Erhan, V. Vanhoucke, and A. Rabinovich. Going deeper with convolutions. In *Proc. of the IEEE Conference on Conference on Computer Vision and Pattern Recognition (CVPPProc. MA.)*, pages 1–9, 2015. 2, 3, 4, 5, 6, 7, 13, 16
- [39] Y. Tang, N. Srivastava, and R. R. Salakhutdinov. Learning generative models with visual attention. In *Proc. of Advances in Neural Information Processing Systems (NeurIPS)*, pages 1808–1816, 2014. 2
- [40] J. K. Tsotsos. *A Computational Perspective on Visual Attention*. MIT Press, 2011. 1
- [41] A. Veit and S. Belongie. Convolutional Networks with Adaptive Inference Graphs. In *Proc. of the European Conference on Computer Vision (ECCV)*, pages 3–18, 2018. 2
- [42] F. Walch, C. Hazirbas, L. Leal-Taixé, T. Sattler, S. Hilsenbeck, and D. Cremers. Image-Based Localization Using LSTMs for Structured Feature Correlation. In *Proc. of the IEEE Conference on International Conference on Computer Vision (ICCV)*, pages 627–637, 2017. 2, 4, 5, 6, 11, 12, 13, 14, 16
- [43] F. Wang, M. Jiang, C. Qian, S. Yang, C. Li, H. Zhang, X. Wang, and X. Tang. Residual Attention Network

- for Image Classification. In *Proc. of the IEEE Conference on Conference on Computer Vision and Pattern Recognition (CVPR)*, pages 6450–6458, 2017. [2](#)
- [44] J. Wang, H. Zha, and R. Cipolla. Coarse-to-Fine Vision-Based Localization by Indexing Scale-Invariant Features. *IEEE Trans. Systems, Man, and Cybernetics, Part B*, 36(2):413–422, 2006. [1](#)
- [45] R. J. Williams. Simple Statistical Gradient-Following Algorithms for Connectionist Reinforcement Learning. *Machine Learning*, 8:229–256, 1992. [2](#)
- [46] S. Xingjian, Z. Chen, H. Wang, D.-Y. Yeung, W.-K. Wong, and W.-c. Woo. Convolutional LSTM Network: A machine learning approach for precipitation nowcasting. In *Proc. of Advances in Neural Information Processing Systems (NeurIPS)*, pages 802–810, 2015. [2](#), [3](#), [4](#)
- [47] K. Xu, J. Ba, R. Kiros, K. Cho, A. C. Courville, R. Salakhutdinov, R. S. Zemel, and Y. Bengio. Show, Attend and Tell: Neural Image Caption Generation with Visual Attention. In *Proc. of the International Conference on Machine Learning, (ICML)*, pages 2048–2057, 2015. [2](#), [3](#), [4](#), [11](#), [12](#), [13](#)
- [48] W. Zaremba, I. Sutskever, and O. Vinyals. Recurrent Neural Network regularization. *CoRR*, 2014. [2](#)
- [49] M. D. Zeiler and R. Fergus. Visualizing and Understanding Convolutional Networks. In *Proc. of the European Conference on Computer Vision (ECCV)*, pages 818–833, 2014. [1](#)
- [50] B. Zhou, A. Lapedriza, J. Xiao, A. Torralba, and A. Oliva. Learning deep features for scene recognition using places database. In *Proc. of Advances in Neural Information Processing Systems (NeurIPS)*, pages 487–495, 2014. [12](#)

A. Detailed Attention Architecture

Figure 5, illustrates the layer selection mechanism. The mechanism receives input h_t from ConvLSTM. It then performs an average pool and an intermediate gate embedding before prediction. We add the Gumbel samples to the predicted logits and perform an *argmax* to select the optimal layer. The gate embedding layer dimension E is much smaller than C . This gate embedding layer helps build a possible representation of incoming features at every LSTM steps, without significantly increasing the network parameters.

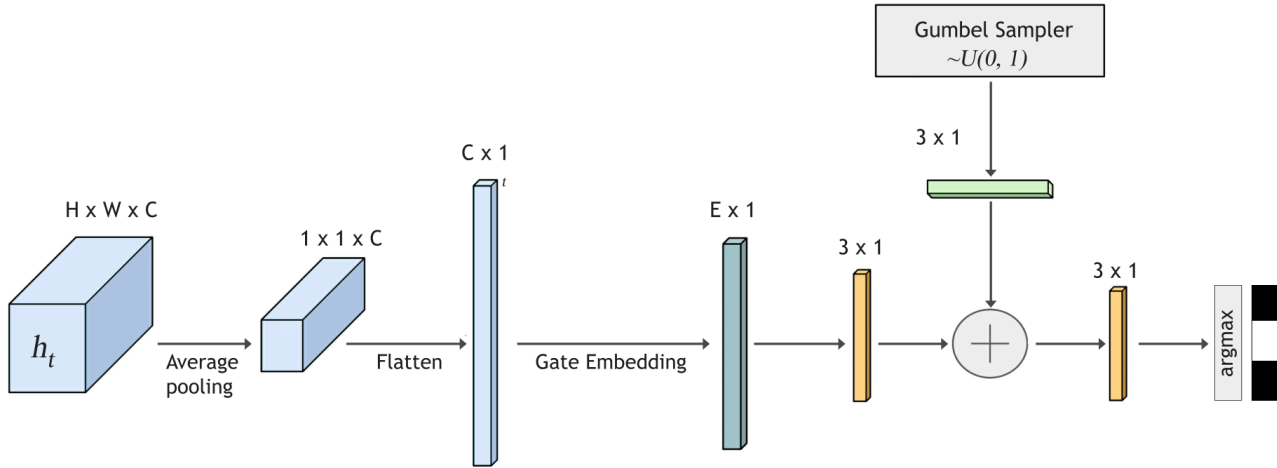


Figure 5: Layer Selection Mechanism.

Figure 6, illustrates the soft attention mechanism. Unlike the soft attention mechanism proposed in Xu *et al.* [47] our's replace fully-connected layers with convolutional layers. Specifically, we used multi-convolutional layers that uses different kernel sizes similar to an inception module. At each time step t , the module receives h_t from ConvLSTM and the selected feature layer F_t . The ConvLSTMs hidden state h_t is first converted to the appropriate channel size of the feature map. We add the embedding h_t and feature layer F_t . Then we apply a non-linearity (Leaky ReLU). After which we compute the attention weights and apply softmax to get the attention map. Then an element-wise multiplication is performed between features and attention map to get the final output of the soft attention module. The Multi-ConvLSTM is applied to attention output. At each time step the LSTM output is used for prediction. In Section suggest convolutional attention and LSTMs yield better results. We did try using fully-connected LSTMs; however, the system consistently failed to pick different locations in the image during successive LSTM steps.

B. Datasets

Cambridge Landmarks [21] A large scale outdoor dataset, containing five outdoor datasets. For our experiments, we only use the four datasets that were used by [21] and [42]. The dataset consists of RGB images. Six degrees-of-freedom camera poses are provided for each image. The dataset was collected using a smart phone, and structure from motion was employed to label each image with its corresponding camera pose.

7-Scenes [36] A small scale indoor dataset, which consists of seven different scenes. These scenes were obtained using Kinect RGB-D camera, and KinectFusion[14] was used to obtain the ground truth. We use the train/test split used by [21] and [42]. Scene contain ambiguous regions, which makes camera localization difficult.

TU Munich Large-Scale Indoor (TUM-LSI) [42] An indoor dataset, which covers an area of two orders of magnitude larger than that covered by the 7Scenes dataset. It consists of 875 training images and 220 testing images. We use the train/test split used by [42]. This is a challenging dataset to localize due to repeated structural elements with nearly identical appearance.

MIT-67 indoor scenes [32] Images taken primarily in four different indoor environments—store, home, public spaces, leisure and working places. The dataset contains 67 categories in total. We used the official train/test split provided by [32]. Each category has 80 training images and 20 testing images.

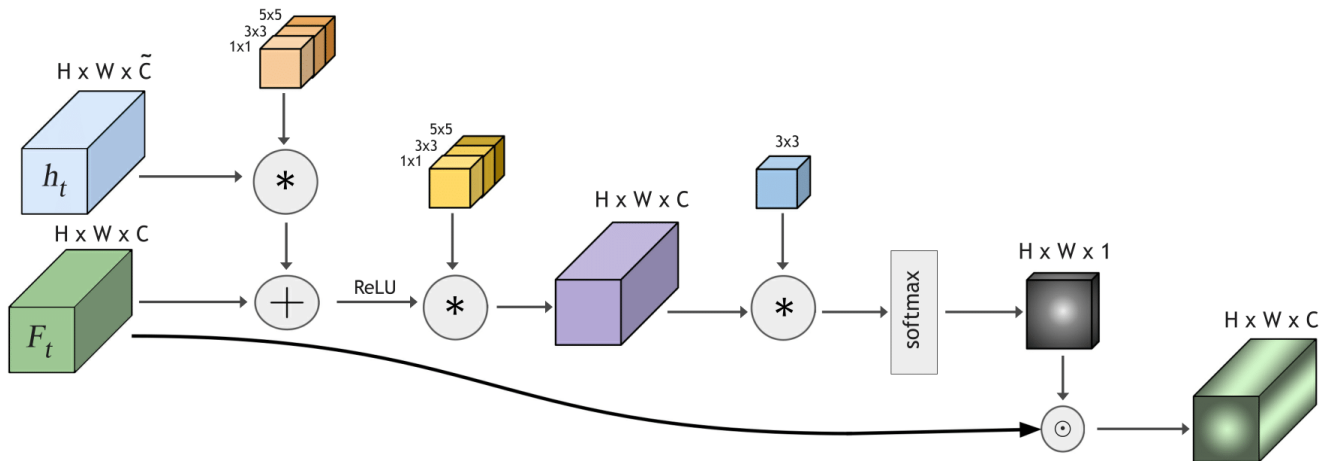


Figure 6: Soft Attention Mechanism.

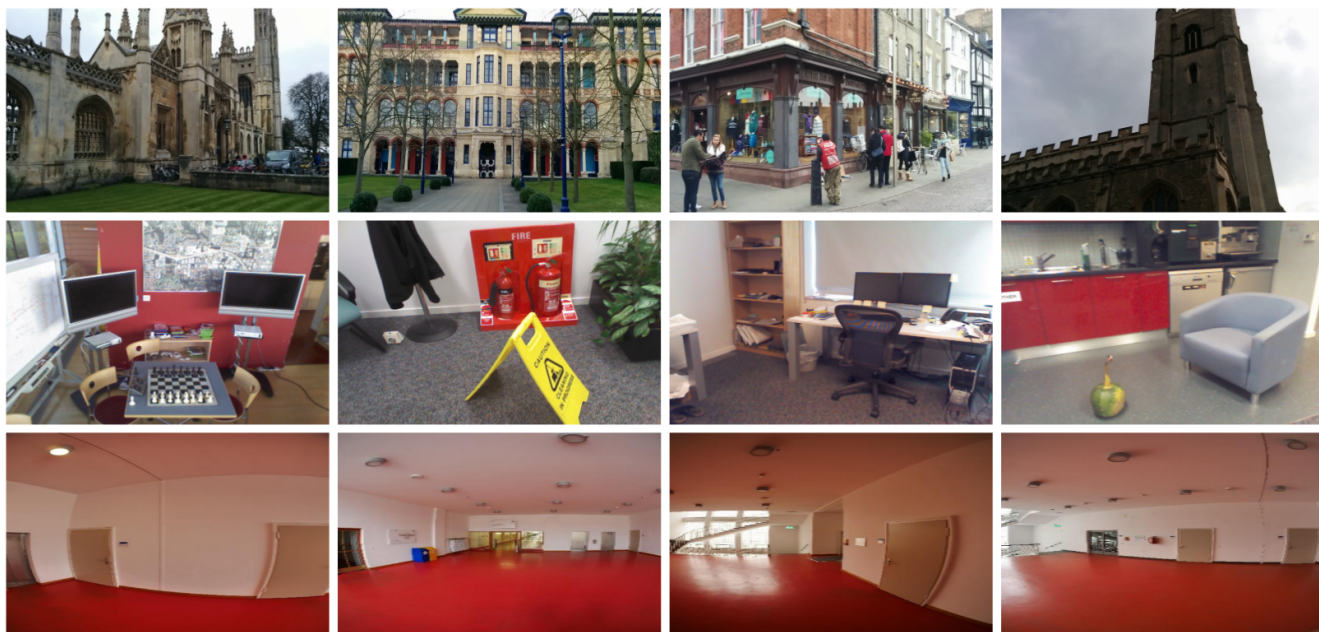


Figure 7: (a) Top row: Cambridge Landmarks Dataset. King's College, Old Hospital, Shop Facade and St. Mary's Church. (b) Middle row: 7-Scenes (subset). Chess, Fire, Office and Pumpkin. (c) Bottom row: TUM-LSI.

C. Extended Implementation details

Similar to [21] and [42], separate mean images were computed for each channel and the images were mean subtracted per channel. For Cambridge Landmarks dataset β value was set between 250 to 2000. For 7-Scenes dataset β value was set between 120 to 750, and for TUM-LSI dataset β value was set to 1000. For indoor scene classification we mean subtract the Places dataset image mean. For both camera pose estimation and indoor scene classification, we used the same pre-trained CNN layers as used by previous methods. We used the original GoogLeNet weights trained on Places¹ [50]. We converted these provided trained network weights to be able to use these in *TensorFlow*. The batch size during training was set to 40. The initial memory states of the LSTM (Memory state c_0 and Hidden state h_0) is typically set to zero. Similar to [47], we

¹<http://places.csail.mit.edu/downloadCNN.html>



Figure 8: MIT-67 Indoor Scene Dataset. (a) Top row: Airport, Auditorium, Concert Hall and Classroom. A network can have a hard time classifying them by just focusing on specific properties, since all of them contain large hallways with chairs. (b) Bottom row: Bookstore, Library, Video Store and Library. This set of images have almost the same structure and objects which makes these scenes very ambiguous.

Dataset	PoseNet [21]	LSTM-PoseNet [42]	Ours	
			Convolutional Spatial Attention	Improvement (meter, degree) %
King’s College	1.66 m, 4.86°	0.99 m , 3.65°	1.39 m, 2.63°	-27.2, +27.6
Old Hospital	2.62 m, 4.90°	1.51 m , 4.29°	3.72 m, 4.24°	-120.5, +6.9
Office	0.48 m, 7.24°	0.30 m , 8.08°	0.64 m, 7.89°	-103.3, +3.2
Stairs	0.48 m, 13.1°	0.40 m , 13.7°	0.48 m, 12.8°	-15.0, +6.5
TUM-LSI	1.87 m, 6.14°	1.31 m , 2.79°	3.93 m, 2.15°	+16, +22.9

Table 4: Median localization error achieved by the convolutional attention model on a subset of camera pose estimation datasets: Cambridge Landmarks, 7-Scenes, and TUM-LSI dataset. Bold values indicate the lowest error achieved for each row.

learn the the initial states. The ConvLSTM hidden size is set to 96.

C.1. Multi-Convolutional Approach

In this section, we describe our motivation for using the multi-convolutional approach. To showcase how we arrived at the proposed approach, we provide evaluation on all three datasets for the pose estimation. We initially started with the same implementation as Xu *et al.* [47] for soft attention, by using fully connected layers. The model ended up overfitting the data and showed poor performance on the test set. Also, the network converged to select only a single spatial feature instead of probing through the other spatial features at different LSTM time-steps. Our first solution was converting fully connected layers into fully convolutional layers. The results for this approach on pose estimation is shown in Table 4. The results shown is quite far from [42] especially on the position, but interestingly error was close to [21].

We found that our model was underfitting the training data. Naively increasing the depth size or kernel size was not showing any significant improvements. Therefore by taking inspiration from the inception module proposed in GoogLeNet

Dataset	PoseNet [21]	LSTM-PoseNet [42]	Ours	
			Multi-Conv. Spatial Attention	Improvement (meter, degree) %
King’s College	1.66 m, 4.86°	0.99 m, 3.65°	0.95 m, 4.11°	+4.04, -12.6
Old Hospital	2.31 m, 5.38°	1.51 m, 4.29°	1.76 m, 4.44°	-16.5, -3.49
Office	0.48 m, 7.24°	0.30 m, 8.08°	0.28 m, 7.52°	+6.67, +6.93
Stairs	0.48 m, 13.1°	0.40 m, 13.7°	0.32 m, 12.7°	+20.0, +9.40
TUM-LSI	1.87 m, 6.14°	1.31 m, 2.79°	1.12 m, 3.66°	+14.5, -2.88

Table 5: Median localization error achieved by the multi-convolutional attention model on a subset of camera pose estimation datasets: Cambridge Landmarks, 7-Scenes, and TUM-LSI dataset. Bold values indicate the lowest error achieved for each row.

[38], we converted each convolutional layer into multi-convolutional layers. We used three convolutional kernels with kernel sizes of 1x1, 3x3 & 5x5 and stacked their final output together. Similarly, in the case of ConvLSTM, we used four convolutional kernels with kernel sizes of 1x1, 3x3, 5x5 & 7x7. Then stacked their final output together for prediction. This approach helped improve results significantly as shown in Table 5. After which we applied our contribution of layer selection mechanism to form layer-spatial attention. The final results for pose estimation is shown in Table 1 in the main paper.

D. Extended results

D.1. Results for Manual Layer Search

In this section, we show an extensive list of classes in MIT-67 indoor scene classification dataset. This table is an extension to the Table 3 from the main main paper. This is provided to showcase how different layers of CNN capture distinctive information that can help further improve the result.

Scene	Layer	Layer	Layer
	3B	4E	5B
Office	33.3	52.3	42.8
Library	65.0	45.0	60.0
Wine Cellar	71.4	76.1	61.9
Fastfood Restaurant	58.8	88.2	70.5
Operating Room	47.3	52.6	36.8
Train Station	85.0	65.0	60.0
Airport-inside	40.0	60.0	75.0
Closet	77.7	88.8	94.4
Game Room	45.0	75.0	80.0
Garage	72.2	77.7	94.4
Dining room	38.8	66.6	77.7
Locker room	66.6	85.7	100.0

Table 6: Indoor scene classification. Mean Accuracy results (%) after applying spatial soft attention to feature maps from different GoogLeNet layers. Top rows show the classes that improve as we look at different layers. Bottom rows show the classes that decrease performance when looking at other layers. Bold values indicate the highest accuracy achieved for each row.

D.2. Results for five Conv-LSTM steps

Dataset	Area or Volume	PoseNet [21]	Bayesian PoseNet [20]	LSTM PoseNet [42]	Ours					Improvement (meter, degree)
					Conv-LSTM Step-1	Conv-LSTM Step-2	Conv-LSTM Step-3	Conv-LSTM Step-4	Conv-LSTM Step-5	
Old Hospital	2000 m ²	2.62 m, 4.90°	2.57 m, 5.14°	1.51 m, 4.29°	1.62 m, 4.11°	1.51 m, 4.02°	1.36 m, 3.95°	1.55 m, 4.46°	1.64 m, 4.20°	+9.93, +7.92
St. Marys Church	4800 m ²	2.45 m, 7.96°	2.11 m, 8.38°	1.52 m, 6.68°	1.62 m, 7.22°	1.59 m, 5.94°	1.42 m, 6.07°	1.49 m, 5.87°	1.58 m, 6.51°	+6.57, +1.64
Office	7.5 m ³	0.48 m, 7.24°	0.48 m, 8.04°	0.30 m, 8.08°	0.29 m, 7.63°	0.29 m, 7.23°	0.29 m, 8.02°	0.29 m, 8.07°	0.30 m, 8.12°	+3.33, +0.74
Stairs	7.5 m ³	0.48 m, 13.1°	0.48 m, 13.1°	0.40 m, 13.7°	0.32 m, 9.98°	0.31 m, 10.5°	0.29 m, 12.0°	0.31 m, 12.0°	0.33 m, 10.9°	+27.5, +12.4
TUM-LSI	5575 m ²	1.87 m, 6.14°	-	1.31 m, 2.79°	1.32 m, 3.82°	1.26 m, 3.69°	0.98 m, 2.74°	1.14 m, 3.33°	1.18 m, 3.68°	+25.1, +1.79

Table 7: Median localization error achieved by our proposed attention model over five-time steps on subset of Cambridge Landmarks, subset of 7-Scenes, and TUM-LSI. Bold values indicate the lowest error achieved for each row. Improvement is reported with respect to LSTM-PoseNet [42].

CNNaug-SVM [35]	S ² ICA [8]	GoogLeNet [38]	Ours					Improvement (%)
			Conv-LSTM Step-1	Conv-LSTM Step-2	Conv-LSTM Step-3	Conv-LSTM Step-4	Conv-LSTM Step-5	
69.0 %	71.2 %	73.7 %	74.5 %	77.1 %	76.0 %	75.4	74.8	+3.4

Table 8: Mean accuracy results for indoor scene classification on MIT-67. The proposed method achieves the highest accuracy (shown in boldface). Improvement is reported with respect to the GoogLeNet [38] baseline.

Camera localization. We did an experimental study for a subset of scenes from camera localization dataset shown in Table 7. We concluded that for the camera position estimation Conv-LSTM step three on average provides the best result.

Indoor Scene Classification. We did an experimental study on MIT-67 indoor scene, shown in Table 8. We concluded that for the Indoor Scene Conv-LSTM step two on average provides the best result.